True Amplitude Migration Using Common-shot One-way Wavefield Extrapolation

Yu Zhang and James Sun
Veritas DGC Inc., Houston, Texas, USA

Carl Notfors
Veritas DGC Inc., Singapore Veritas DGC Inc., Singapore

Samuel H. Gray*
Veritas DGC Inc., Calgary, Alberta, Canada
Sam_Gray@Veritasdgc.com

Norman Bleistein
Colorado School of Mines, USA

Guanquan Zhang
Chinese Academy of Sciences, China

ABSTRACT

Summary

We analyze the amplitudes produced by shot-record migration using one-way wavefield extrapolation in a $v(z)$ medium. By comparing these amplitudes with those produced by true-amplitude Kirchhoff migration, we identify the amplitude and phase errors that come from a standard implementation of migration by one-way wavefield extrapolation. Next, we present a new formulation of shot-record migration that maintains its high fidelity in imaging complex structures and has correct dynamic behavior for a $v(z)$ velocity. In numerical tests we show that true-amplitude common-shot migration produces an asymmetric impulse response, and we give a physical explanation for this behavior.

Introduction

Until recently, Kirchhoff migration has been used for most 3-D prestack migrations, primarily because of its versatility and efficiency. The demands of imaging increasingly complex geological structures, however, have spurred a demand for increased imaging fidelity. This has led to the growing popularity of imaging methods that handle more than the single arrival that Kirchhoff migration is capable of handling conveniently. Such methods include finite-difference migration, which allows for an unlimited number of arrivals. In this paper, we concentrate on one-way wavefield extrapolation, paying particular attention to its amplitude and phase behavior.

The standard formulation of finite-difference migration (Claerbout, 1985) consists of two parts. The first part is the downward continuation of the wavefields from the source and receiver locations using a split "wave equation." The second part is the application of an imaging condition, and one standard imaging condition is the division of the downward continued receiver wavefield by the downward continued source wavefield at each image point. Unfortunately, the one-way “wave equations” used in the downward continuation are not equivalent to the acoustic wave equation whose behavior they are designed to mimic. This mismatch leads to a migrated wavefield that lacks correct amplitude and phase behavior, even though it is kinematically correct. By expressing the downward continued wavefields asymptotically, we are able to compare the imaged wavefield with the reflection coefficient produced by true amplitude Kirchhoff migration. Our comparison leads to a corrected equation for the upgoing and downgoing wavefields. When these corrections are applied, the migration produces images whose amplitudes and phases agree with true-amplitude Kirchhoff migration.

Theory

We begin with a layered velocity ($v(z)$) earth and 3D common-shot migration. Given an acoustic wave-field p with source excitation at $\vec{x}_s = (x_s, y_s, 0)$ and $t = 0$,

$$\left(\frac{\partial^2}{v^2\partial t^2} - \frac{\partial^2}{\partial z^2} - \frac{\partial^2}{\partial x^2} - \frac{\partial^2}{\partial y^2}\right) p(\vec{x};t) = \delta(\vec{x}-\vec{x}_s)\delta(t), \qquad (1)$$

we record the surface data Q:

$$p(\vec{x}_r, z=0;t) = Q(\vec{x}_r;t). \qquad (2)$$

According to Bleistein et al.’s (2001) work on inversion, the true-amplitude common shot Kirchhoff migration formula is (Zhang, et al., 2000)

$$R \sim \int i\omega \frac{\sqrt{\cos\alpha_{s0}\cos\alpha_{r0}}}{v_0} \sqrt{\frac{\psi_s \sigma_s}{\psi_r \sigma_r}} e^{i\omega(\tau_s+\tau_r)} \hat{Q}(\vec{x}_r;\omega) d\vec{x}_r d\omega, \qquad (3)$$

where ψ and σ are in-plane and out-of-plane geometrical spreading terms and α_{s0} and α_{r0} are surface angles at shot and receivers, respectively (see Figure 1); hat denotes temporal Fourier transform.

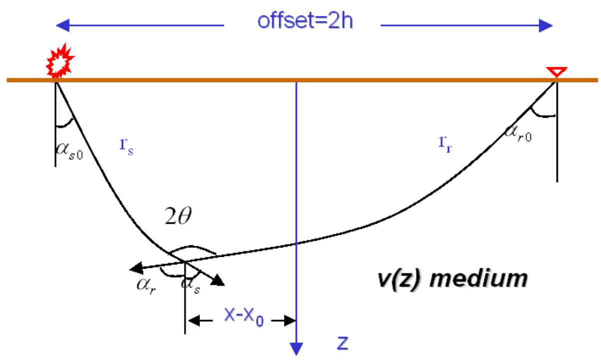

Fig. 1: Ray paths in a $v(z)$ medium

For conventional common-shot migration, we downward continue both shot and receiver wavefields, D and U, which we assume to satisfy the following equations (Claerbout, 1985)

$$\begin{cases} \left(\dfrac{\partial}{\partial z} + \Lambda\right) D(x, y, z; t) = 0, \\ D(x, y, z = 0; t) = \delta(\vec{x} - \vec{x}_s)\delta(t), \end{cases} \tag{4}$$

and

$$\begin{cases} \left(\dfrac{\partial}{\partial z} - \Lambda\right) U(x, y, z; t) = 0, \\ U(x, y, z = 0; t) = Q(x, y; t). \end{cases} \tag{5}$$

Here Λ is the square-root operator. To produce the image, we use the imaging condition

$$R(\vec{x}) = \int \frac{\hat{U}(\vec{x}; \omega)}{\hat{D}(\vec{x}; \omega)} d\omega. \tag{6}$$

For a $v(z)$ medium, Zhang et al. (2001a) give an asymptotic expression for the one-way wave fields:

$$\hat{D}(\vec{x}; \omega) \sim \frac{i\omega}{2\pi} \sqrt{\frac{\cos\alpha_s}{\psi_s \sigma_s}} e^{-i\omega\tau_s} \tag{7}$$

and

$$\hat{U}(\vec{x}; \omega) \sim \iint \frac{i\omega}{2\pi} \sqrt{\frac{\cos\alpha_r}{\psi_r \sigma_r}} e^{i\omega\tau_r} \hat{Q}(\vec{x}_r; \omega) d\vec{x}_r. \tag{8}$$

Substituting (7) and (8) into (6), we obtain

$$R(\vec{x}) \sim \iiint \sqrt{\frac{\cos\alpha_r \psi_s \sigma_s}{\cos\alpha_s \psi_r \sigma_r}} e^{i\omega(\tau_s + \tau_r)} \hat{Q}(\vec{x}_r; \omega) d\vec{x}_r d\omega. \tag{9}$$

Comparing (9) with (3), we conclude that the algorithm (4-6) cannot provide a true amplitude image; even the phase term $i\omega$ is missing from (9).

In Zhang et al. (2001b), we give a remedy to correct the amplitude for constant velocity, but an additional correction term needs to be applied for a $v(z)$ medium. Here we formulate the following modified phase-shift migration algorithm which gives the true amplitude common-shot migration result for $v(z)$ velocity. Its generalization to a completely heterogeneous $v(x, y, z)$ acoustic medium appears in Zhang et al. (2002).

Let $\tilde{p}(k_x, k_y; \omega)$ denote the spatial-temporal Fourier transform of the wavefield $p(x, y; t)$. Instead of solving for D and U, we propose to solve for pressure fields p_D and p_U, which satisfy the following equations (Zhang, 1993) and boundary conditions:

$$\begin{cases} \left(\dfrac{\partial}{\partial z} + \lambda - \gamma\right) \tilde{p}_D(k_x, k_y, z; \omega) = 0, \\ \tilde{p}_D(k_x, k_y, z = 0; \omega) = \dfrac{1}{2\lambda} e^{i(k_x x_s + k_y y_s)}, \end{cases} \tag{10}$$

and

$$\begin{cases} \left(\dfrac{\partial}{\partial z} - \lambda - \gamma\right) \tilde{p}_U(k_x, k_y, z; \omega) = 0, \\ \tilde{p}_U(k_x, k_y, z = 0; \omega) = \tilde{Q}(k_x, k_y; \omega), \end{cases} \tag{11}$$

where

$$\lambda = i \frac{\omega}{v} \sqrt{1 - v^2 \frac{k_x^2 + k_y^2}{\omega^2}}$$

and

$$\gamma = \frac{v_z}{2v} \frac{\omega^2}{\omega^2 - v^2 (k_x^2 + k_y^2)}.$$

Also, we modify the imaging condition (6) to be the quotient of the wavefields p_D and p_U:

$$R(\vec{x}) = \int \frac{\hat{p}_U(\vec{x}; \omega)}{\hat{p}_D(\vec{x}; \omega)} d\omega. \tag{12}$$

It can be proved that equations (10) and (11), together with imaging condition (12), are equivalent to equation (3) in the high-frequency limit.

Numerical tests

Fig. 2 (left) shows 3-D migrated impulse responses along the center inline from a trace with three 7.5Hz Ricker wavelets at depth 1000m, 2000m and 3000m. The source is at crossline 121 and receiver at crossline 141; trace spacing is 50m in both inline and crossline directions. The medium velocity is 2000m/s. According to the theory of true-amplitude Kirchhoff migration (i.e., from equation (3), using expressions for α, ψ, and σ from Bleistein et al. (2001)), the common-shot migration weight is $z\frac{r_s}{r_r^2}$. This expression for the amplitudes of the impulse responses is asymmetric in r_s and r_r, with a bias on the receiver side. *Fig. 2* (right) shows the numerical peak amplitudes along the impulse responses, in good agreement with the theoretical prediction.

The Kirchhoff weight for 3-D common-offset migration is $z\left(\frac{r_s}{r_r} + \frac{r_r}{r_s}\right)\left(\frac{1}{r_r} + \frac{1}{r_s}\right)$, which is symmetric in r_s and r_r. The asymmetry of the impulse response for true amplitude common-shot migration appears to violate physical intuition. (Shouldn't the formula be the same if source and receiver locations are interchanged?) We resolve this paradox by noting that, in true amplitude migration, the migration weight is used to compensate for the ray density at all the image locations. *Fig. 3* shows that, for constant velocity, common-offset migration, the subsurface ray density on the left and right dipping reflectors are the same. In common-shot migration (*Fig. 4*), the situation is different. Since the travel distances for the reflections from the left and right reflectors are essentially the same, their geometrical spreading losses are equal. If the reflectivities on the left and right reflectors are also the same, the amplitudes of reflections from both dipping reflectors are identical. On the other hand, from *Fig. 4* we see that the subsurface ray density is greater on the shot side than on the receiver side. Therefore, to obtain balanced migrated amplitudes (which are proportional to reflectivity), the migration weight needs to take this ray density difference into consideration. Some detailed algebra shows that the common-shot migration weight compensates exactly for the ray density difference.

Fig. 5 shows a 2-D true amplitude migration result from a single shot over four flat reflectors with density-only contrasts in a medium with velocity $v(z) = 2000 + 0.3z$. The input data (top panel) was generated by applying geometrical spreading to equal-amplitude Ricker wavelets with traveltimes computed analytically. The bottom left panel is the migrated shot record. The peak amplitudes along the four migrated reflectors are shown in the bottom right panel. Aside from the edge effects and small amounts of jitter caused by interference with wraparound artifacts, the $v(z)$ true amplitude common shot migration recovers the reflectivity accurately.

A word of warning about true-amplitude common shot migration: the formulation resulting in equation (3) assumes an areal array of receivers for each shot, covering an infinitely extensive recording surface. Clearly, 3-D marine streamer data, with a relatively narrow swath of long cables, violates this assumption. As a result, equation (3) should be modified in practice to account for an acquisition geometry that is partly 2-D and partly 3-D. In the limiting case of a single streamer, the migration formula (3) becomes a 2.5-D formula, with phase factor $\sqrt{i\omega}$, not $i\omega$. In practice, our wavefield extrapolation true-amplitude formula needs to match this phase factor.

Conclusions

Migrations based on one-way wavefield extrapolation offer the potential of greater structural imaging quality than single-arrival Kirchhoff migration. However, the standard formulation of such migrations, e.g. finite-difference migration, produce incorrect migrated amplitudes. By comparing these amplitudes with those produced by true-amplitude Kirchhoff migration, we have, in effect, calibrated these migration methods, correcting their amplitude and phase behavior.

References

Bleistein, N., Cohen, J. K., and Stockwell, J. W., 2001, Mathematics of multidimensional seismic inversion: Springer.

Claerbout, J., 1985, Imaging the earth's interior: Blackwell Scientific Publication, Inc.

Zhang, G., 1993, System of Coupled Equations for Up-going and Down-going waves, Acta Math. Appl. Sinica, 16:2, 251-263.

Zhang, Y., Gray, S., and Young, J., 2000, Exact and approximate weights for Kirchhoff migration: 70th Ann. Mtg., Soc. Expl. Geophys., Expanded Abstracts, 1036-1039.

Zhang, Y., Gray, S. and Young, J., 2001a, True-amplitude Common-offset, Common-azimuth *v(z)* Migration, Journal of Seismic Exploration (accepted).

Zhang, Y., Sun, J., Gray, S., Notfors, C. and Bleistein, N., 2001b, Towards Accurate Amplitudes for One-way Wavefield Extrapolation of 3-D Common Shot Records, 71st Ann. Mtg., Soc. Expl. Geophys (Workshop).

Zhang Y., Zhang, G. and Bleistein, N., 2002, Theory of true amplitude common-shot migration, 72nd Ann. Mtg., Soc. Expl. Geophys.

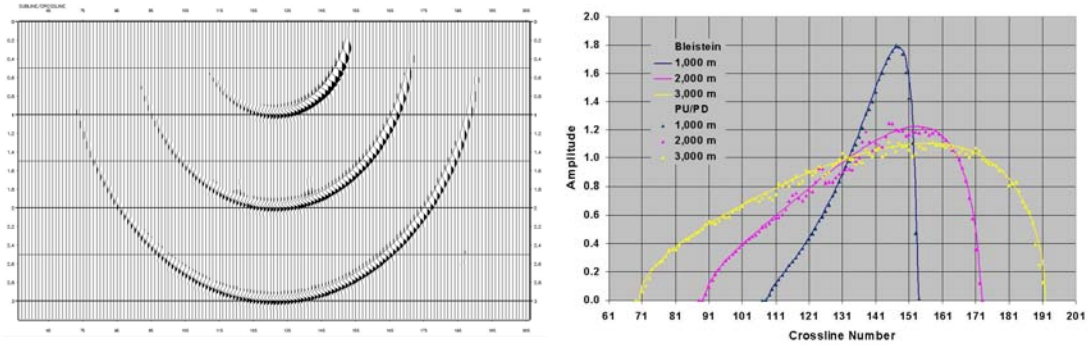

Fig. 2: Left: 3-D phase-shift migrated impulse responses along the center inline. The shot is at crossline 121 and receiver at crossline 141. Right: Amplitudes of the 3-D migrated impulse responses.

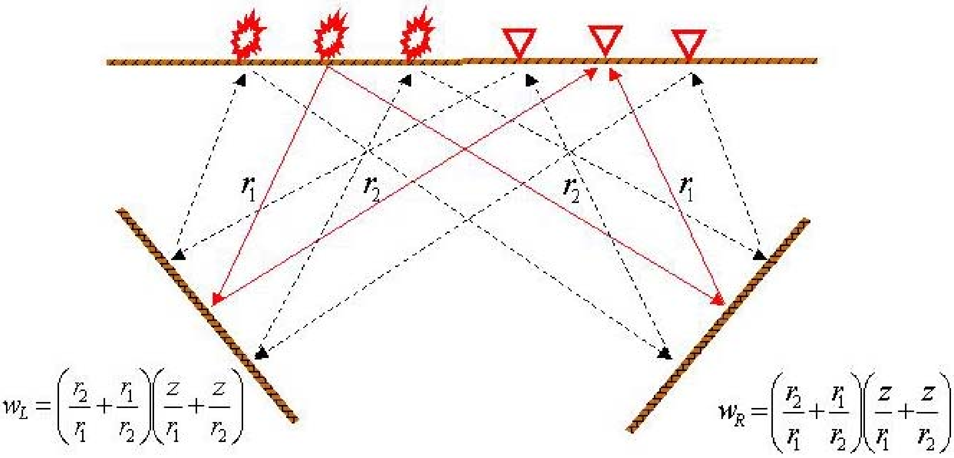

Fig. 3: Ray density for common-offset migration onto dipping reflectors.

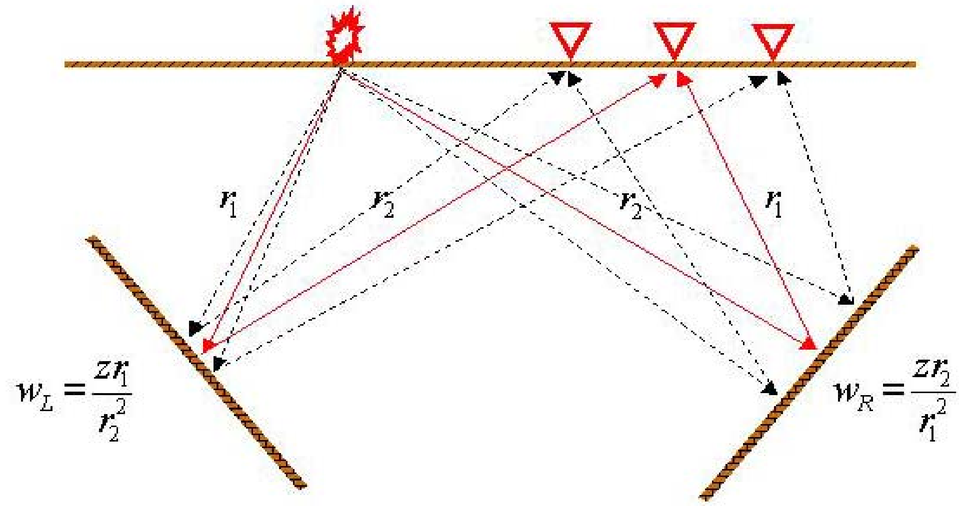

Fig. 4: Ray density for common-shot migration onto dipping reflectors.

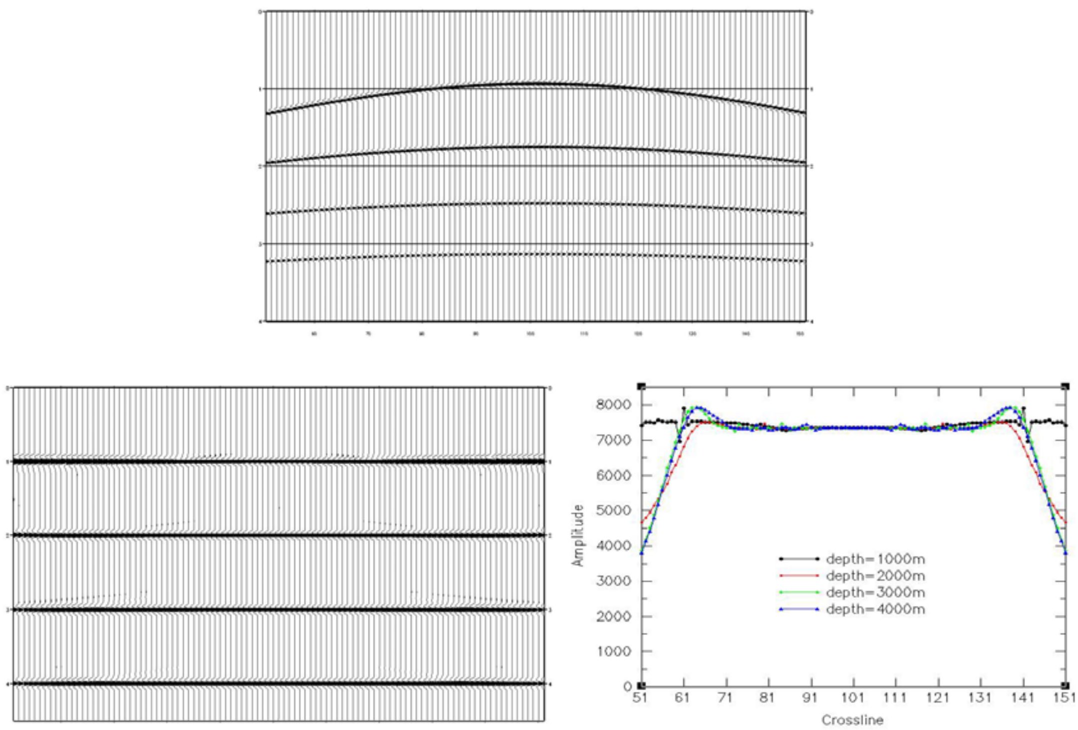

Fig. 5: Top: 2-D shot record from four flat reflectors in a medium with velocity $v(z) = 2000 + 0.3z$. Bottom left: migrated shot record. Bottom right: Peak amplitudes along the migrated reflector.